JOURNAL OF MATERIALS SCIENCE 13 (1978) 1015–1025

Rain erosion behaviour of polymethylmethacrylate

WILLIAM F. ADLER
Materials Science Section, Effects Technology Inc., Santa Barbara, California 93111, USA

STEPHEN V. HOOKER
Department of Material Science and Engineering and the Materials and Molecular Research Division, University of California, Berkeley, California 94720, USA

Mass loss, optical transmittance and the microscopic erosion sequence have been monitored for polymethylmethacrylate exposed to a 2.54 cm h^{-1} rainfall of 1.8 mm diameter water drops at an impact velocity of 222 m sec^{-1}. Initial drop impacts produced well-defined fracture patterns consisting of a circular area free of damage surrounded by an annulus containing a dense array of fine, short cracks together with a sparse distribution of deeper fractures initiated along surface scratches. Continued exposure to the rainfield produced crack grown and crack intersections at sites of fracture annuli overlap followed by crevice growth as these fracture systems were enlarged by a hydraulic penetration mechanism. An extensive network of subsurface fractures continued to be produced within the expanding cavities with longer exposures. The transient stress distributions generated during a water drop impact on polymethylmethacrylate are considered in terms of their potential for producing circumferential fractures.

1. Introduction

The rain erosion behaviour of polymethylmethacrylate (PMMA) is described from the onset of damage due to the initial water drop impacts to large scale mass removal at a single impact velocity of 222 m sec^{-1}. When a 1.8 mm water drop strikes the PMMA target at 222 m sec^{-1}, the resulting damage is in the form of an annular region of circumferential cracks. The central undamaged zone ranged from 0.60 to 0.75 mm in diameter and the outer diameter ranged from 0.80 to 1.5 mm. A typical ring crack formation is shown in Fig. 1.

Single water drop impacts have been described by Engel [1] and Fyall [2]. According to Engel, circumferential cracking forms around the point of impact of an impinging, spherical water drop due to the tensile stresses that are produced when the compressive impact stress forms a cup-shaped cavity in the material. A breaking out of material from the surface should be observed as a result of the rapid radial outflow of water over the raised ridges of the fine circumferential cracks that have formed [1]. The impact conditions in the experiments reported by Engel are for an average 1.9 mm water drop striking PMMA at 222 m sec^{-1}. Fyall's experiments [2] were for a 2 mm water drop impinging at 276 to 298 m sec^{-1}. At these velocities a smooth annular depression is observed to occur outside the central undamaged zone with circumferential cracking seen beyond this depressed zone. Fyall provides an explanation similar to that of Engel except that he allows for permanent set in the deformed regions XLA and BMY in Fig. 2. He explains that before lateral outflow occurs the surface AB in Fig. 2 is compressed to A'B'. The sides of the depression XA' and YB' would then be in tension and the tensile stresses would be set up over XD and YE resulting in circumferential cracking. Fyall's measurements of the change of lengths from XA and YB to the deformed state show that any residual tensile strain is very small. The surface returns to AB but the small permanent

set induced in XA′ and YB′ gives the profiles XLA and BMY.

Profilometer traces along a diameter of a number of the circumferential crack patterns shown in Fig. 1 for an impact velocity of 222 m sec^{-1} indicated the presence of an annular depressed zone which ranged in depth from 0.2 to 0.4 μm. Single water drop impact experiments have also been carried out in our ballistic range facility for 2 mm drops impacting PMMA at 250 to 450 m sec^{-1}. Profilometer traces show the depth of the annular depressed zone increasing. At 300 m sec^{-1} the mean depth is 1.5 μm for a 2 mm diameter drop, in accord with Fyall's measurements.

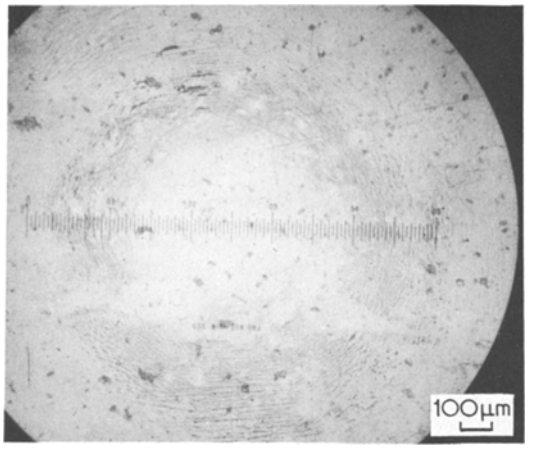

Figure 1 Typical annular circumferential crack pattern on PMMA when impacted by a 1.8 mm water drop at 222 m sec^{-1}.

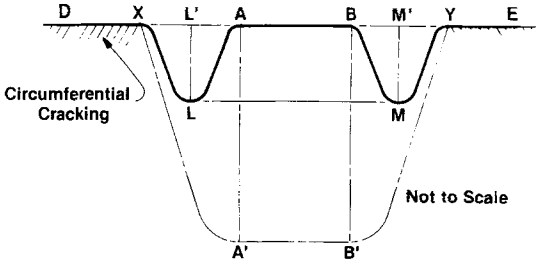

Figure 2 Engel/Fyall mechanism for circumferential crack formation in PMMA (taken from [2]).

Higher velocity impacts on PMMA have been described using water jets instead of spherical drops. Field *et al.* [3] have embarked on a programme to demonstrate the quantitative as well as the qualitative similarities between a spherical water drop impact and a water jet. At the lower impact velocities in their investigation they show a direct correspondence between a Talysurf profilometer trace for one of Fyall's PMMA specimens and the damage due to a water jet collision. The Cambridge investigators [3–6] have described the damage modes in thin and thick specimens of PMMA subjected to jet impacts from 290 to 1200 m sec^{-1}. The smooth annular depressions surrounding the central undamaged region in Fyall's experiments were observed for impact velocities up to 500 m sec^{-1} when deep ring cracks would originate within the annular depressed zone. The circumferential cracks outside the annular depressed region were found to be almost perpendicular to the surface but tended to grow parallel to the surface with increasing radial distance from the initial point of impact. The depth of the cracks decreased with radial distance, but the average depth was around 10 μm. Using multiple beam interferometry, Bowden and Brunton [4] found that at each fracture there is a small step in the surface which is oriented so that the vertical face of the step faces in toward the centre of impact. The height of the mismatch is around 2000 Å. During the impact a radial force acts on the step face due to lateral outflow from the collapsing water drop. This interaction is sufficient to chip material out of the surface along the line of fracture as seen in Engel's early micrographs [1] and in our observations of the early stages of the erosion process in a variety of materials in addition to PMMA.

The nature and progression of the damage produced by multiple water drop interactions which eventually lead to measurable mass removal will be described for an impact velocity near the threshold for the formation of coherent ring fractures. The change in the character of the damage produced by a single drop impact as a function of impact velocity has been described above, however a corresponding detailed analysis of multiple drop interactions and the manner in which material is eventually removed at these higher velocities does not appear to be available.

The results reported here were obtained from erosion tests conducted in the AFML/Bell rotating arm erosion facility, Buffalo, New York, and the AFML rotating arm, Wright–Patterson Air Force Base, Dayton, Ohio. Both facilities are calibrated

for a standard rainfield of 2.54 cm h^{-1} consisting of a mean water drop diameter of 1.8 mm. This calibration however does not imply that the number of drop impacts on a unit area of the specimen's surface after equal exposure increments is the same in each facility. The distance the drops fall from a position of zero vertical velocity and the rotational velocity of the arm determine the number of drops impacted. Calculations for an impact velocity of 222 m sec^{-1} indicate that specimens exposed to this rainfield in the AFML/Bell facility receive 8.8 impacts cm^{-2} sec^{-1} and 10.35 impacts cm^{-2} sec^{-1} in the AFML facility for normal impacts on the exposed face of the specimen. The specimens used in the work reported here were made from Rohm and Haas Plexiglas II UVA. The specimen dimensions were 3.80 cm × 2.22 cm × 0.95 cm and 8.25 cm × 2.22 cm × 1.27 cm in the AFML/Bell facility and 3.80 cm × 1.27 cm × 0.635 cm for the AFML rotating arm.

2. Analysis of single drop impacts

The circumferential fracture annulus shown in Fig. 1 can be due to the Engel/Fyall mechanisms shown in Fig. 2 as well as due to stress waves propagating outward from the impact site. The circumferential fractures may be a combination of both of these fracture-producing mechanisms: direct deformation of the contact zone and stress wave propagation. In order to investigate these possibilities further the transient stress states within the target material will be evaluated based on an idealized model of a liquid drop striking a material surface [7]. In order to realize the loading the PMMA experiences upon collision with a single water drop, various features of the transient stress distributions will be summarized. First of all it may be as well to understand the way in which a water drop loads the surface.

The sequence of events which takes place when a spherical liquid drop strikes a rigid plane have been reviewed [7]. In summary, the drop quickly loads the surface to a maximum pressure which is released near the time when lateral outflow (collapse of the drop onto the surface) takes place. The lateral outflow jetting of liquid at a velocity several times the impact velocity moves in a direction parallel to the surface. Its direction is dependent on the extent to which the contact area between the drop and the surface is depressed during the pressure build-up phase. The pressure then subsides to the stagnation pressure of the liquid. The temporal and spatial development of the pressure applied to the surface and the magnitude of the maximum pressure are still unsettled in the current literature. For a 1.8 mm water drop impacting at 222 m sec^{-1} the rise time to maximum pressure is on the order of 0.25 μsec and the relaxation period can be somewhat longer. The stagnation pressure is reached within 1 μsec.

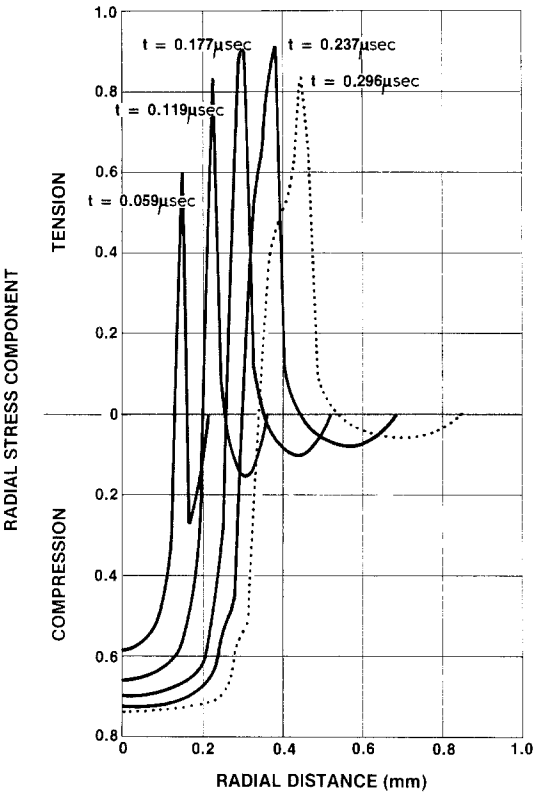

Figure 3 Temporal development of the radial stress component in PMMA 5 μm below the surface for a 1.8 mm water drop impacting at 222 m sec^{-1}.

In the stress wave analysis a uniform distribution of pressure acts within a rapidly expanding circular region on the surface of the specimen up to the time at which lateral outflow is assumed to take place. While the solution does not accurately represent the details of the pressure loading phase, it does provide a good approximation for the propagation and relative magnitude of the transient stresses generated during the initial stage of the collision. Based on the water drop impingement damage observed for PMMA, the critical stress locations appear to lie in the surface layer of the specimen surrounding the impact site. The circum-

ferential crack annuli originate by the imposition of tensile radial stresses.

The temporal development of the transient radial stress component at a depth of 5 μm below the surface is shown in Fig. 3. As explained in [7] the solution displays a singularity in the region surrounding the location of the Rayleigh wave front which presents computational difficulties. The stress distributions evaluated slightly below the surface are quite representative of those on the surface and the computational difficulties are avoided. For the stress calculations in Fig. 3, radial outflow is assumed to occur when the expanding contact radius between the drop and the surface reaches a value of 0.308 mm. After the radius at which radial outflow occurs is reached the applied pressure subsides. However, the radial stress component will continue to propagate. The decreasing magnitude of the normal pressure will only influence the amplitude of the propagating stresses generated after the time lateral outflow occurs.

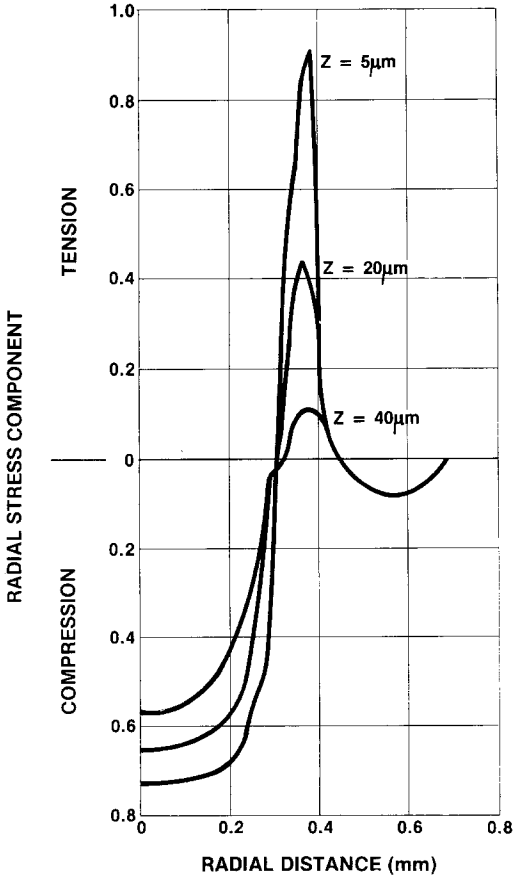

Figure 4 Variation of the radial stress component with depth at the time drop collapse is assumed to take place for a 1.8 mm water drop impacting PMMA at 222 m sec^{-1}.

The contact circle over which the normal pressure acts will continue to expand, but at a different rate from that stipulated in the stress calculation, to radii beyond that at which lateral outflow takes place, possibly up to 0.5 times the drop radius. The continuation of the calculation beyond the critical radius is included in Fig. 3. The critical contact radius for lateral outflow is selected based on observations of the nature of the damage produced by single drop collisions on the surface of PMMA, as shown in Fig. 1. The variation of the radial stress distribution with depth into the specimen is shown in Fig. 4 at the time the loaded contact zone reached 0.308 mm.

The magnitude of the applied uniform pressure distribution is normalized to unity in Figs. 3 and 4. The magnitude of the uniform pressure can be estimated from a one-dimensional shock wave analysis which, for the impact conditions used here, yields a value of 242 MPa [7]. Upon multiplying the normalized values of the radial stress components in Figs. 3 and 4 by the magnitude of the applied pressure, the values of the radial stress components are found.

The stress distributions in Figs. 3 and 4, along with evaluation of the other stress components, or principal stresses, evaluated for various times throughout the half-space, provide insight into the critical stress conditions which can initiate damage in the specimen. From Fig. 3 it is seen that an average radial tensile stress of approximately 120 MPa acts over a radial distance of 0.15 mm for 0.09 μsec. At a depth of 20 μm (Fig. 4) the magnitude of the average radial stress is roughly 60 MPa and acts over essentially the same spatial and temporal dimensions. Although the effects of the impact are quite localized, the spatial dimension over which the tensile stress acts increases with radial distance in the vicinity of the surface. Its slowly decreasing magnitude and longer duration are still effective in producing circumferential fractures at radial distances beyond those indicated in Fig. 3. While the magnitude of the stresses generated may not be accurate due to the uncertainty in the form of the pressure distribution, the temporal development of the stress waves is probably representative of the physical impact conditions for the relatively low impact velocity of 222 m sec^{-1}. Calculations based on the theory of elasticity indicate that the maximum displacement of the region under the contact zone will be approximately 10 μm for an applied pressure of 242 MPa. The

numerical computations would support the view that circumferential fractures arise due to the direct deformation of the material surrounding the compressed region under the contact zone and at larger radial dimensions due to the development and propagation of tensile stress waves propagating to shallow depths away from the impact site. The radial extent of the fractures and the fracture depth observed for water drop impacts on PMMA are consistent with this analysis.

3. The erosion process

The sequence of events leading to measurable mass removal from the surface of PMMA exposed to the rain environment will be described from the initial impact of isolated water drops to the final stages of large-scale material removal. These observations are based on incremental exposures of the PMMA specimens to the rainfield in the rotating arm facilities. The exposure times are specified in terms of the computed number of drop impacts the specimen receives per square centimetre of exposed surface. All of the results described are for drop collisions normal to the face of the specimen.

3.1. Single water drop fracture modes

In the absence of surface scratches, the initial impact by a 1.8 mm diameter water drop at 222 m sec^{-1} produced a ring crack pattern (an annulus composed of discontinuous fractures). The central region, whose diameter ranged from 0.60 to 0.75 mm, was free from both surface and subsurface damage. An annulus of fine discontinuous fractures surrounded the central core with outer diameters ranging from 0.80 mm to as large as 1.5 mm. The larger dimensions may be due to anomalously large drops compared to the mean diameter of 1.8 mm for the rainfields in the rotating arm facilities. These initial fractures appeared to form by a brittle mechanism with no evidence of concurrent microplastic response. The circumferential crack distribution is shown in Fig. 1.

Two types of fractures are found within the annular crack pattern formed on PMMA by the initial impact. One type is composed of straight line fractures formed along the paths of scratches which pass through the annulus tangential to the circular impact symmetry. A network of fine scratches were present despite careful surface preparation and handling. This scratch-initiated fracture mode is very sensitive since topologically enhancing illumination such as Nomarski interference contrast or oblique illumination was required for scratch detection in the absence of subsequent impact enlargement of these scratches. These preferential fractures preceded lateral outflow jetting, since systematic pitting of only the exterior crack edge occurred at sites of single impacts. Bowden and Brunton [4] examined the outer fracture profiles produced by supersonic water jets and established that the exterior edge was displaced upward several thousand angstroms to present a small but abrupt step toward the impact site. A similar profile exists in the band of fractures examined here based upon the directions of the shadows cast under oblique illumination microscopy. The scratch-initiated fractures may penetrate to significant depths, as illustrated by the initial water drop impacts shown in Fig. 5. The outward inclination of these fractures is consistent with the stress distribution calculated for subsonic and low supersonic drop impacts on both glasses and plastics.

The second type of fracture in the crack annulus is composed of a dense band of very short, wavy cracks as shown in Fig. 5 for the initial impact. The fracture lengths range from 5 to 50 μm with the length increasing but the fracture density decreasing as the distance from the impact site increases. Although the cracks are easily resolved with an optical microscope, neither an observable fracture depth nor a detectable surface opening could be seen. The height discontinuity associated with these fractures is significantly smaller than the straight line scratches, since very little lateral outflow pitting was observed. In contrast, the circumferential fractures reported by Bowden and Brunton [4] for supersonic jet impacts possessed both measurable depth of 10 μm and openings of a micron or greater.

3.2. Water drop interactions

The initial impacts on the PMMA surface due to both types of fractures produced a sparse field of isolated water drop imprints until the onset of sequential interaction at an impact density of approximately 12 impacts cm^{-2}. Three types of sequential impact geometry could be reconstructed from the sites of multiple particle impacts. First, for a second impact of approximately concentric geometry, the least probable event, the resultant damage retained the circular symmetry but the density and magnitude of damage was increased

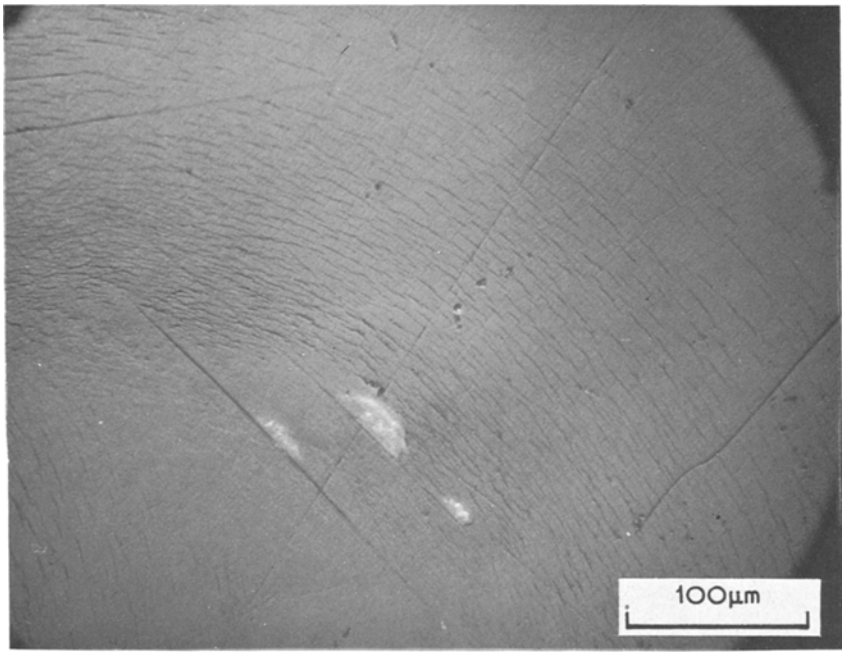

Figure 5 Detail of scratch initiated penny-shaped cracks and disjoint array of circumferential fractures characterstic of a single water drop impact on PMMA at 222 m sec^{-1}.

significantly. Second, for an impact in which the impact sites were separated by 0.5 to 1.0 times the central undamaged zone diameter, two primary locations for enhanced damage are observed. The first location is the central zone of the second overlapping impact in the region where it covers the preceding annular fracture zone producing enlarged straight fractures. This damage arises due to the hydraulic stresses generated by penetration of the water during the second impact into the enlarged scratches within the annular fracture zone formed by the initial impact. The original sites of lateral outflow fracture and pitting provide the most favourable structure for subsequent fluid penetration. The second location for enhanced damage occurs at the sites of annuli overlap. The dense array of nonpreferential fractures formed by the second impact interacts with the initial fractures to form intersecting fracture arrays. Although these intersecting fractures did not possess optically resolvable widths, crevice formation occurred preferentially in these networks during further exposure, indicating that fluid impact could effectively penetrate such structures. A size distribution was noted for which the largest fractures tended to form at the perimeter of the second impact array away from the original impact. And finally, the most probable case for sequential impacts at separation distances greater than the diameter of the central undamaged zone overlap occurred primarily at a single site between the annular fracture arrays. This overlap produced a large network of intersecting fractures analogous to the zones of overlap described above for closely spaced impacts. The dimensions of the preferential fractures, those coherently formed along scratch paths, tended to be larger for the wider spaced impacts, presumably because midway between the impact centres these structures underwent two successive lateral outflow impacts. The magnitude of the radial tensile stresses is also greater at these radial distances as shown in Fig. 3. Scratch enlargement also occurred effectively within the central zone of the subsequent impact when the fluid overlapped the outer portion of the original annular array. The largest fractures resulted at preferential fractures within the original band when these underwent initial enlargement by a lateral outflow impact and then fluid penetration. Widths for these fractures ranged from 1 to 3 μm, which were two to three times the widths generally observed at non-intersecting sites. Discontinuous intersecting fracture arrays were formed also as described above. It was observed that the central undamaged zone for the initial impact impeded, but did not prevent, the formation of annular fracture damage in this region, as the second impact propagated through the initial annular fractures. Bowden and Brunton [4] have reported an overlapping supersonic jet experiment which qualitatively resembles the sequence described: the fracture enhancement beneath the second impact (several mm deep),

the impedance of fractures through the first central impact zone, and the tendency for lateral outflow opposite to the initial impact are all better defined. However, because each impact produced mm deep damage, both in the central zone as well as in the surrounding annulus, the multiple impact sequence was less important for exposure to jets; however for the conditions described here, it was a requirement for crevice formation during the incubation period.

Observations of a later impact in the neighbourhood of previous drop damage zones indicate that the annular fracture zones of the first two to four impacts produce very fine, intersecting networks of fractures, which are not well sealed at the surface. Subsequent collision with a drop whose contact area overlaps these intersecting fractures opens crevices with widths ranging to 5 μm or more and extended lengths. However, unlike inorganic glasses in which repeated drop impacts at 222 m sec^{-1} produce a jagged and forked system of continuous deep cracks which span the exposed surface, arrays of shorter ($< 200\,\mu$m) crevices were produced in PMMA due to an apparent capacity for localized strain [8]. The propagation of these crevices formed along the circumferential fracture arrays and maintained favourable alignment with the dynamic stress distributions along the lines of intersecting fractures, as shown in Fig. 6. Fracture openings are now rapidly and selectively enlarged. The formation of cracks and crevices with appreciable widths (greater than 1 μm) completed the initiation stage; the hydraulic penetration mechanism dominated the subsequent erosion process. The wider openings are now rapidly and selectively enlarged via the original annular fracture paths.

3.3. Material removal

During subsequent rainfield exposure equivalent to 90 impacts cm^{-2}, the onset of macroscopic erosion was observed, as shown in Figs. 7 and 8. At this stage the surface was rapidly becoming covered with a dense maze of fine cracks and crevices together with the formation and growth of large cavities (diameters greater than 1 mm). Although the impact sequence could not be traced precisely, due to the large number of sequential impacts, the numerous changes of direction and the plastic deformation at the crevice edges of the original single and double impact sites effectively persisted due to enhancement by hydraulic penetration. A high density of conchoidal fractures were formed at cavities, within crevices and along scratches (shown in Fig. 5). The combination of the strain associated with the extensive surface fractures together with a limited capacity for strain at high strain rates is believed responsible for the brittle behaviour of the exposed surface. The existence of such embrittlement is suggested more clearly in the rain erosion of polycarbonate in which the

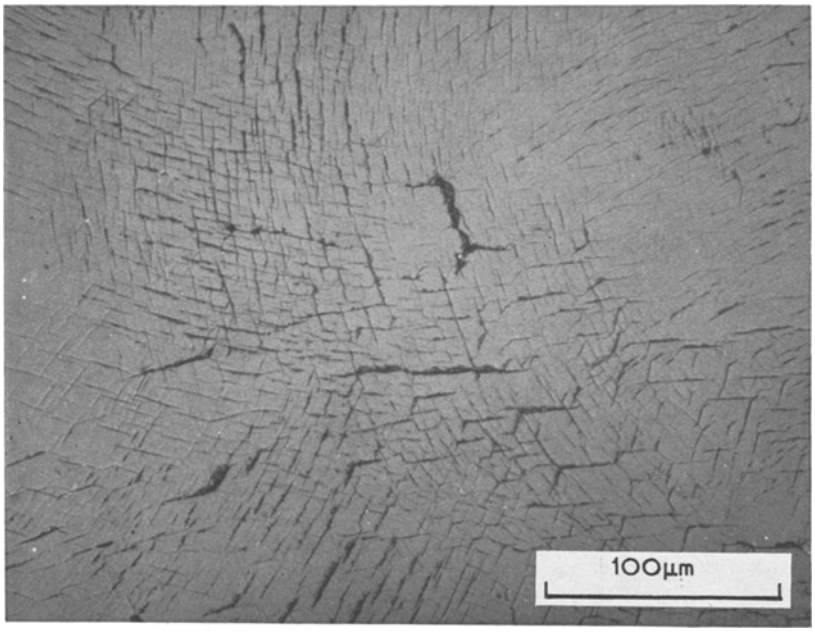

Figure 6 Crevice formation at sites of intersecting circumferential fractures associated with two or more water drop impacts.

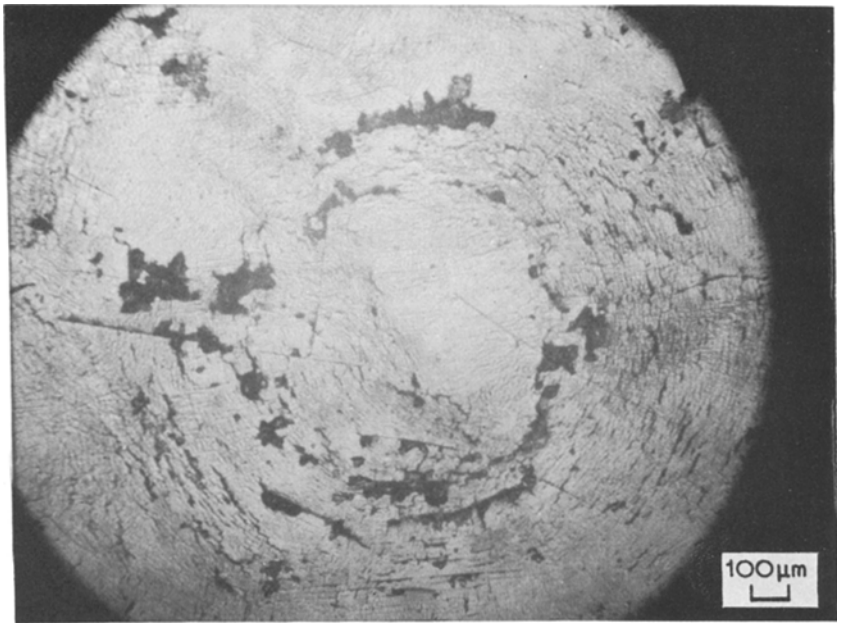

Figure 7 General overview of the early stage development of erosion pits.

initial drop impacts produce ductile ripples whereas the subsequent impacts primarily introduce fracture. Thus selective fracture growth rather than a more dense distribution of fine surface fractures results. Consequently the selective formation of much larger cavities from the interacting fracture networks would be influenced by the contributions from local embrittlement at the fracture site (the larger structural dimensions of which both facilitate fluid penetration and increase the local stress distributions) and perturbations in the interfacial pressure distribution as the drop contact zone expands over the irregular surface. This more destructive mechanism was responsible for rapid growth of the large cavities, since the cavity walls were composed primarily of overlapping arrays of semicircular fractures (radii perhaps 50 to 75 μm). The increased dimensions of these cavities then permitted direct drop impact against the wall fractures accelerating the erosion process. Continued exposure produces a more uniform distribution of erosion pits obscuring the original impact sites as

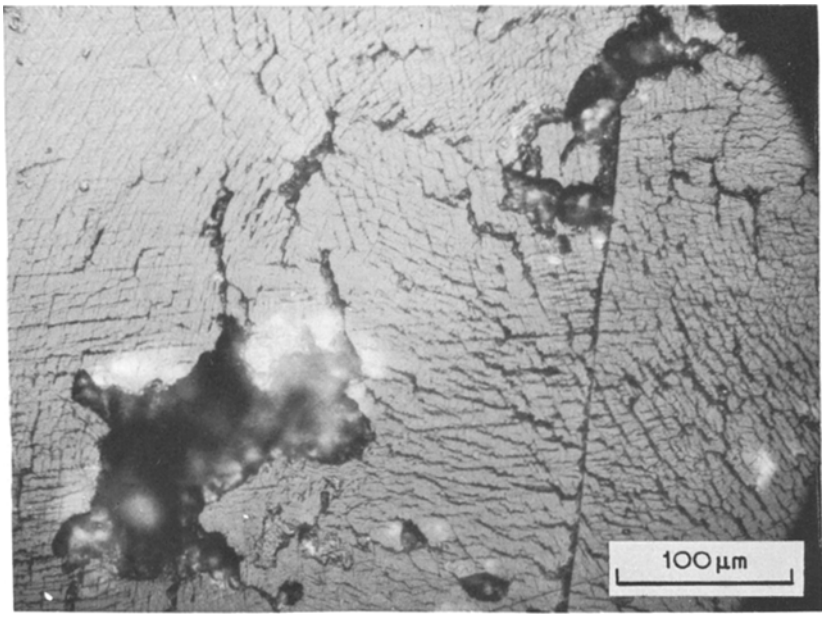

Figure 8 Detail of erosion pits and evidence of hydraulic penetration of the water in an impacting drop on cracks, crevices and small pits at the initial stage of the material removal process.

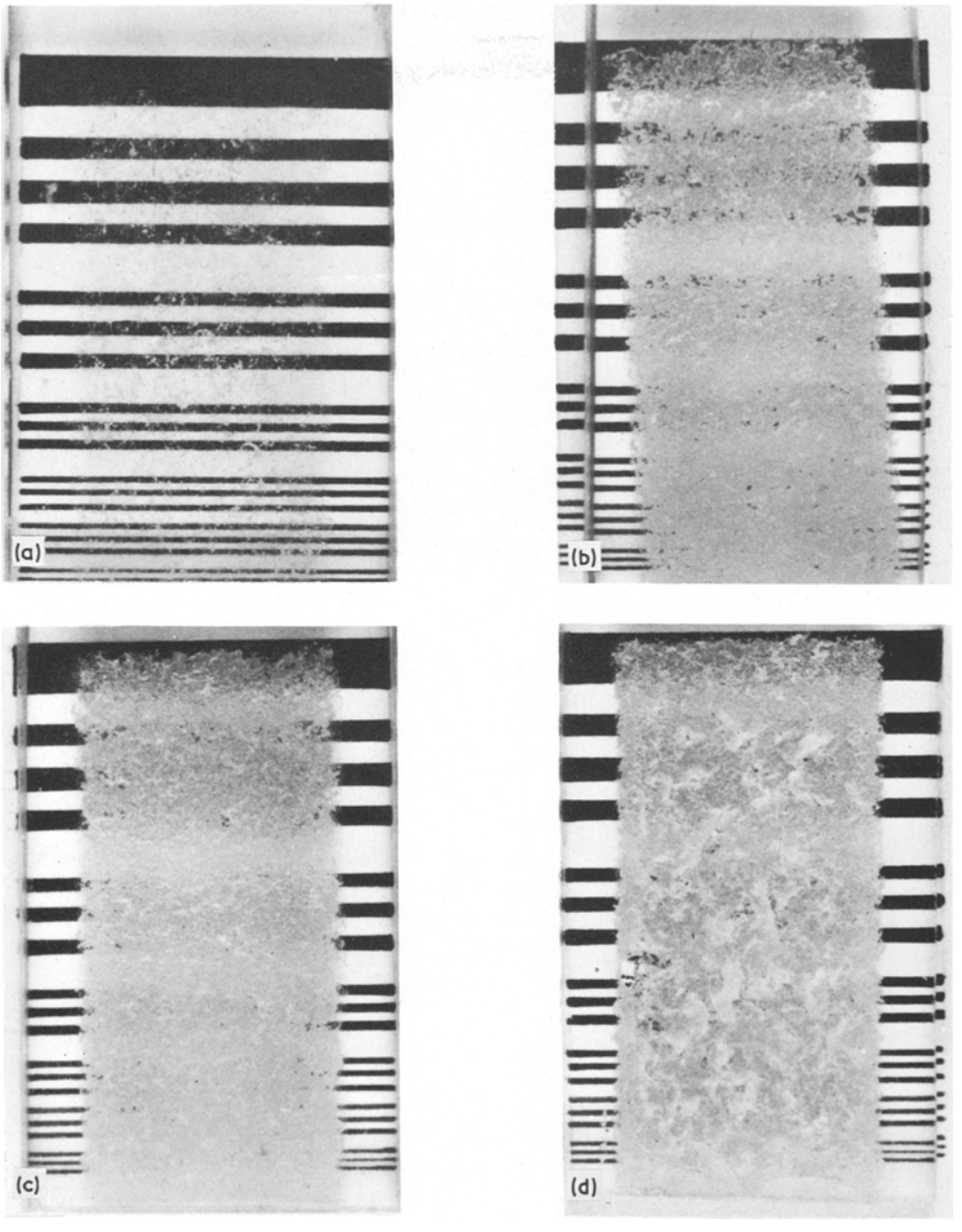

Figure 9 Optical resolution pattern viewed through eroded specimens of PMMA after impacting 1.8 mm water drops at 222 m sec^{-1}. (a) PM-1, 265 impacts cm^{-2}; (b) PM-2, 530 impacts cm^{-2}; (c) PM-3, 795 impacts cm^{-2}; (d) PM-4, 1060 impacts cm^{-2}.

an increasing proportion of irregularly shaped cavities appear whose structures bear no apparent relationship to the surrounding eroded structure.

The macroscopic erosion of PMMA is seen in Fig. 9 for exposure times which result in large-scale material removal. A Model 14 Cary Recording Spectrophotometer was used to evaluate the transmittance for these specimens over a wavelength range from 0.5 to 2.1 μm. The optical degradation is indicated in Fig. 10. The specimen labelled PM-0 represents the reference transmittance measurement for an uneroded specimen. The percent degradation is seen to be fairly uniform over the entire range of wavelengths. A 20% reduction in transmittance occurs after 265 impacts cm^{-2}, and the transmittance is essentially zero somewhat before the specimen receives 530 impacts cm^{-2}.

Another test series provided mass-loss measure-

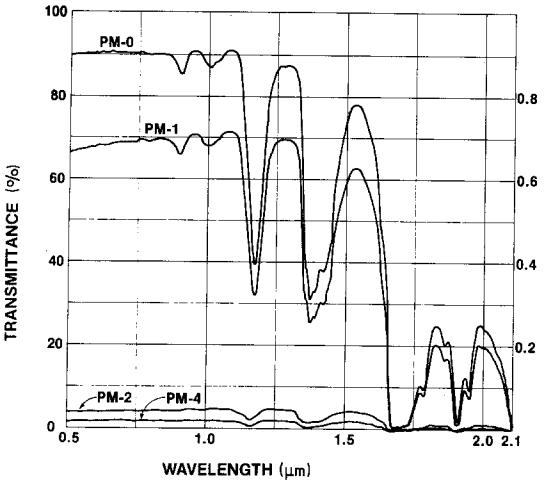

Figure 10 Optical transmittance loss for eroded PMMA specimens shown in Fig. 9.

ments. The same specimen was given consecutive incremental exposures to the rain environment in the AFML/Bell rotating arm facility up to the time when the specimen's surface was eroded to a depth of a millimetre or more. The mass of the specimen was recorded in milligrams after each exposure. The cumulative mass loss was determined in this way and normalized with respect to the actual exposed area of the specimen's surface. Triplicate test specimens were used in this test series. The cumulative mass loss per centimetre squared is plotted as a function of the computed values of the number of drop impacts in Fig. 11. The duration of the incubation period does not exhibit the variability which may be thought to prevail due to the random surface scratch distribution representative of the initial surface condition of the specimens used. The microscopic observations of the progressively-eroded specimens confirm the general character of the mass-loss curve which indicates that continually larger pieces of material are removed from the surface as the exposure time increases. A steady state of material removal was not achieved for these specimens even though more than 1 mm of material was removed when the tests were terminated.

4. Conclusion

Water drop impacts produce identifiable imprints on the surface of PMMA specimens at subsonic velocities which are representative of normal aircraft flight conditions. A strong interaction was found to occur between surface scratches and the transient stresses generated and lateral outflow jetting associated with drop impingement. Progression of the erosion process for PMMA has been traced in some detail for an impact velocity of 222 m sec^{-1}. This detailed investigation of PMMA serves two purposes. It is of interest for the information obtained concerning the erosion process for materials which are more resistant to water drop impact damage at subsonic velocities when the direct effects of each impact are not at all obvious. The random damage gener-

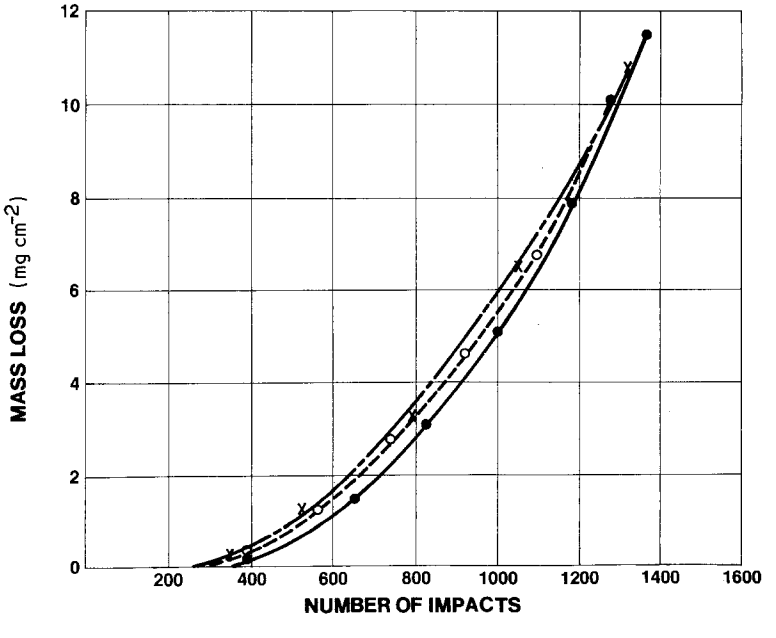

Figure 11 Mass loss as a function of exposure to the rain environment for three PMMA specimens impacting 1.8 mm water drops at 222 m sec^{-1}.

ation observed in these materials can be related to the known multiple impact conditions to which they were exposed as derived from this study of PMMA. Observations of damage progression in PMMA due to higher velocity water drop collisions appear warranted.

Acknowledgement

This research was supported by the Air Force Materials Laboratory under Air Force Contract No. F33615-73-C-5057.

References

1. O. G. ENGEL, *J. Res. Nat. Bur. Stand.* **54** (1955) 51.
2. A. A. FYALL, Proceedings of the Second Meersburg Conference on Rain Erosion and Allied Phenomena, edited by A. A. Fyall and R. B. King (Royal Aircraft Establishment, Farnborough, UK, 1967).
3. J. E. FIELD, J. J. CAMUS, D. A. GORHAM and D. G. RICKERBY, Proceedings of the Fourth International Conference on Rain Erosion and Associated Phenomena, edited by A. A. Fyall and R. B. King (Royal Aircraft Establishment, Farnborough, UK, 1974).
4. F. P. BOWDEN and J. H. BRUNTON, *Proc. Roy. Soc.* **A263** (1961) 433.
5. F. P. BOWDEN and J. E. FIELD, *ibid* **A282** (1964) 331.
6. J. H. BRUNTON, *Phil Trans. Roy. Soc.* **A260** (1966) 79.
7. W. F. ADLER, *J. Mater. Sci.* **12** (1977) 1253.
8. W. F. ADLER and S. V. HOOKER, *Wear* (to be published).

Received 28 January and accepted 24 October 1977.